Interfacial Charge-Transfer Absorption: 3. Application to Semiconductor−Molecule Assemblies†

Carol Creutz,*,‡ Bruce S. Brunschwig,*,§ and Norman Sutin*,‡

Chemistry Department, Brookhaven National Laboratory, Upton, New York 11973-5000, and Beckman Institute, California Institute of Technology, Mail Code 139-74, 1200 East California Boulevard, Pasadena, California 91125

Received: June 23, 2006; In Final Form: August 17, 2006

Interfacial charge-transfer absorption (IFCTA) provides information concerning the barriers to charge transfer between molecules and the energy levels of a metal/semiconductor and the magnitude of the electronic coupling and could thus provide a powerful tool for understanding interfacial charge-transfer kinetics. Here we utilize a previously published model (*J. Phys. Chem. B* **2005**, *109*, 10251) to predict the energetics of IFCTA spectra for semiconductors and compare literature observations to these predictions for n-type semiconductors (largely TiO_2). In contrast to metals, where IFCTA has been only rarely observed, new absorption features due to IFCTA are common for semiconductors such as TiO_2. At issue is whether the electron accepting states in the TiO_2 are localized or delocalized over the conduction band.

I. Introduction

There is presently much effort directed toward characterizing and modeling interfacial charge transfer from molecular species to metals and semiconductors.[1] Thermal electron transfer to/from semiconductor electrodes depends on the carrier density.[2−4] For the case of bulk and nanocrystalline n-type semiconductors the kinetics of both electron photoinjection and back-reaction in dye−TiO_2[5−8] and other n-type metal oxide[9−13] assemblies have been investigated revealing a complex, not yet well understood series of processes. Understanding of molecular electron-transfer reactions has been enhanced through studies of the electronic spectroscopy of molecular donor−acceptor pairs. This area has been most broadly explored for molecular systems (particularly mixed-valence systems)[14−17] for which the band maxima and integrated intensities of binuclear transition-metal complexes,[18−21] ion pairs,[22,23] and organic redox couples[24−28] have been compared with activation barriers and rates for thermal electron-transfer reactions.[29] Such a spectroscopic approach would seem to offer a powerful probe of solute or adsorbate interactions with metal and semiconductor materials or electrodes, especially for nanoparticle systems where the relative surface areas are very large. Indeed optical charge transfer between metal adatoms and CdS and ZnO semiconductor electrodes[30] and between adsorbed ferrocyanide ion[5,31,32] or catechol[33−37] and TiO_2 nanoparticles has been reported. In addition, optical charge-transfer transitions between the conduction band and the particle surface (edge) states have been reported for CdSe,[38] InP,[39] and GaSe[40] nanoparticles.

Interfacial charge-transfer absorption (IFCTA) from solute metal ions to metallic electrodes was predicted by Hush in 1968,[17,41,42] although, to our knowledge, no such absorption bands have been reported.[43] Since both semiconductors and metals possess closely spaced occupied electronic levels and closely spaced unoccupied levels a common framework (with due attention to the differences in the properties of the two kinds of materials) is appropriate for their interfacial charge-transfer processes.[44] As developed by Hush, the interfacial charge-transfer bands are expected to be extremely weak and to lie at long wavelengths (in some cases in the near-infrared or infrared regions) thus making their observation experimentally very challenging. The recent emergence of metal and semiconductor nanoparticles provides a new opportunity to study molecule−interface charge-transfer absorption spectra; the nanoparticles have many sites for adsorption of molecular donors/acceptors so that the probability of charge-transfer absorption is increased relative to comparable adsorption on a bulk material. Furthermore, it is experimentally more straightforward to examine nanoparticle solutions than bulk solute/adsorbate interfaces.

We recently proposed a semiclassical model for IFCTA to metals and semiconductors that takes into account the fact that, unlike molecules, both semiconductors and metals possess closely spaced occupied electronic levels and closely spaced unoccupied levels so that a common framework is appropriate for describing their interfacial charge-transfer processes.[44] In addition, we have compared the features expected for such interfacial charge-transfer absorption for the bulk material and for nanoparticles of metals.[43] The present contribution considers the features expected for such interfacial charge-transfer absorption features for a semiconductor bulk material and for its nanoparticles. We use semiclassical expressions for optical electron-transfer processes that are based on Fermi's golden rule but with the density of states (Franck−Condon factor) of the redox couple treated within the Marcus framework.[44] In the following sections we first introduce recently developed expressions for optical electron transfer between a molecule and a semiconductor, then consider the intensity of such transitions, their reorganizational parameters, and differences expected for bulk and nanoparticulate semiconductors. Finally we consider

† Part of the special issue "Arthur J. Nozik Festschrift".

* Authors to whom correspondence should be addressed. E-mail: ccreutz@bnl.gov, bsb@caltech.edu; sutin@bnl.gov

‡ Brookhaven National Laboratory.

§ California Institute of Technology.

10.1021/jp063953d CCC: $33.50
Published on Web 10/20/2006

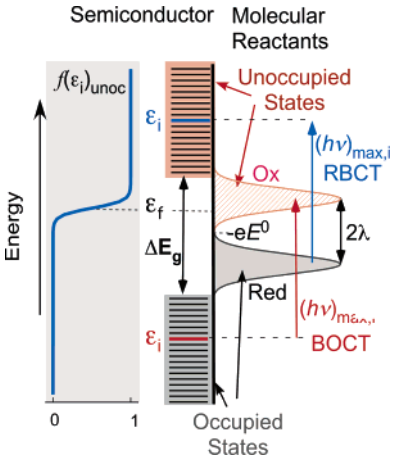

Figure 1. Distribution functions for molecular reactants and a semiconductor with gap ΔE_g. At the left, the electron unoccupancy factor, $f(\epsilon_i)_{unoc} = 1 - f_{oc}(\epsilon_i)$, is depicted.

spectra predicted for molecule semiconductor assemblies and compare these predictions with literature observations.

II. Model for Interfacial Charge-Transfer Absorption with n-Type Semiconductors

Spectroscopic Considerations. Consider a molecule in contact with an n-type semiconductor. In principle, thermal charge transfer to and from the conduction-band (CB) or valence-band (VB) electronic levels B of a semiconductor and those of a molecular electron donor (reductant, Red) or electron acceptor (oxidant, Ox) are both possible. Thus two light-induced electron-transfer processes are expected: An electron may be promoted from an occupied level of the reductant to a vacant level of the semiconductor conduction band or from an occupied level of the semiconductor valence band to an oxidant.

$$\text{Red-B}_{\text{CB}}(\ ) \xrightarrow{h\nu_{\text{RBCT}}} \text{Ox-B}_{\text{CB}}(\text{e}^-) \quad (1)$$

$$\text{Ox-B}_{\text{VB}}(\text{e}^-) \xrightarrow{h\nu_{\text{BOCT}}} \text{Red-B}_{\text{VB}}(\ ) \quad (2)$$

Photoinduced charge transfer to and from the semiconductor levels is entirely analogous to charge-transfer absorption within and between molecules, except that the semiconductor levels form two bands of closely spaced levels (separated by an energy gap) rather than energetically well separated molecular orbitals. To emphasize that a band of levels is involved, we denote optical charge transfer from an electron donor as reductant-to-band charge transfer (RBCT) and to an electron acceptor as band-to-oxidant charge transfer (BOCT).

For semiconductors, the bands of filled levels (valence band) and unoccupied levels (conduction band) are separated by an energy gap ΔE_g (Figure 1). As is outlined in Figure 2, ΔG_i^0 for optically induced electron transfer from an electron donor to the *i*th level in the conduction band of an n-type semiconductor (which is the class of systems most frequently studied) is given by

$$\Delta G_i^{\,0}(\text{RBCT}) = -e(E_i^{\text{CB}} - E^\circ) = \epsilon_i^{\text{CB}} - e(E_{\text{bot}}^{\text{CB}} - E^\circ) \quad (3)$$

where E° is the potential of the redox couple, E_i^{CB} and $E_{\text{bot}}^{\text{CB}}$ are the effective potentials of the semiconductor for electron transfer to the *i*th level of the conduction band and to the bottom level of the conduction band, respectively, and ϵ_i^{CB} is the difference

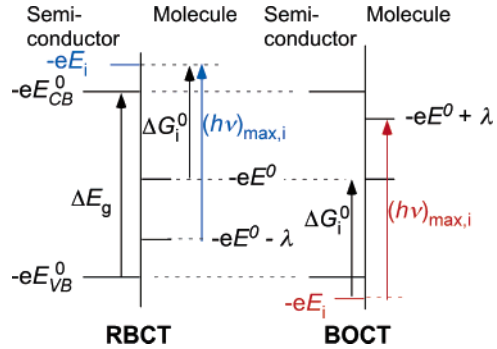

Figure 2. Energetics of RBCT and BOCT for a semiconductor with ΔE_g separating the top of the valence band and the bottom of the conduction band.

between the energy of the *i*th level and the bottom level of the conduction band. Similarly, ΔG_i^0 for optically induced electron transfer from the *i*th level (state) of the valence band to an electron acceptor is given by

$$\Delta G_i^{\,0}(\text{BOCT}) = e(E_i^{\text{VB}} - E^\circ) = -\epsilon_i^{\text{VB}} + e(E_{\text{top}}^{\text{VB}} - E^\circ) \quad (4)$$

where E_i^{VB} and $E_{\text{top}}^{\text{VB}}$ are the effective potentials of the semiconductor for electron transfer from the *i*th level of the valence band and from the highest (top) level of the valence band, respectively, and ϵ_i^{VB} is the difference in energy between the *i*th level (state) of the valence band and the top of the valence band. As defined here, $\epsilon_i^{\text{VB}} \leq 0$ and $\epsilon_i^{\text{CB}} \geq 0$. RBCT absorption should comprise contributions from charge transfer to all unoccupied levels of the conduction band, while BOCT absorption will have contributions from all the occupied valence-band levels. The total observed absorbance is then the sum of the contributions from all of the transitions to (from) the individual levels. The absorption profile for each individual transition is Gaussian.[21]

As previously discussed,[44] the semiclassical model in which the Fermi level of the semiconductor is assumed to lie in the band gap so that the Fermi−Dirac distribution over the energy levels can be replaced by a step function leads to the following expressions for ϵ_ν/ν

$$\left(\frac{\epsilon_\nu}{\nu}\right)^{\text{RBCT}} = \int_0^{+\infty} \rho_i^{\text{CB}} \left(\frac{\epsilon_\nu}{\nu}\right)_{\text{max},i} \times \exp\left[-\frac{(\lambda - h\nu + \epsilon_i^{\text{CB}} - e(E_{\text{bot}}^{\text{CB}} - E^0))^2}{4\lambda k_{\text{B}}T}\right] \mathrm{d}\epsilon_i \quad (5)$$

$$\left(\frac{\epsilon_\nu}{\nu}\right)^{\text{BOCT}} = \int_{-\infty}^{0} \rho_i^{\text{VB}} \left(\frac{\epsilon_\nu}{\nu}\right)_{\text{max},i} \times \exp\left[-\frac{(\lambda - h\nu - \epsilon_i^{\text{VB}} + e(E_{\text{top}}^{\text{VB}} - E^0))^2}{4\lambda k_{\text{B}}T}\right] \mathrm{d}\epsilon_i \quad (6)$$

where ρ_i^{CB} and ρ_i^{VB} are the densities of states (DOS) of the conduction and valence bands, respectively, and λ is the reorganization energy. The maximum value of ϵ_ν/ν for a transition to level *i* is given by[21,45]

$$\left(\frac{\epsilon_\nu}{\nu}\right)_{\text{max},i} = 2\pi^3 \frac{|\mu_{12,i}|^2}{[3 \times 10^3 \ln(10) c\sqrt{\pi\lambda k_{\text{B}}T}]} \quad (7)$$

where $\mu_{12,i} = \langle \Psi_1 | \mu | \Psi_2 \rangle$ is the transition dipole moment, μ is

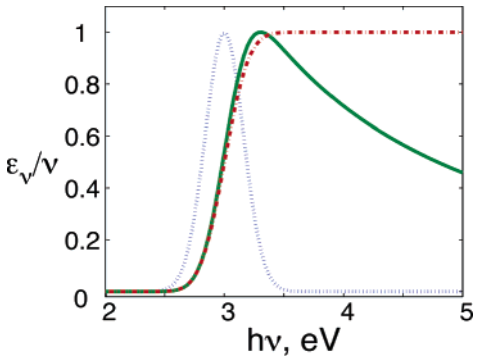

Figure 3. Relationship between the Gaussian component in the semiconductor−molecule charge-transfer transition (dotted blue line) and the overall absorption profile for the energy-independent transition dipole moment (dash−dotted red line) and for Mulliken−Hush coupling at constant $H_{12}r$ (eq 9, solid green line). The parameters used were: $\lambda = 0.5$ eV, $\Delta G° = 2.5$ eV, $T = 298$ K. The semiconductor DOS was assumed constant.

the electric dipole moment operator, and c is the speed of light. The transition dipole moment is related to H_{12}, the electronic coupling between the molecular species and the electronic levels of the band

$$\mu_{12,i} = (H_{12}er/\nu_{\max})_i \tag{8}$$

where r is the distance over which electron transfer occurs. Equation 8 can be combined with eq 7 to give

$$\left(\frac{\epsilon_\nu}{\nu}\right)_{\max,i} = \frac{7.0 \times 10^2 H_{12}{}^2 r^2}{(\nu_{\max,i})^2\sqrt{\lambda k_B T}} \tag{9}$$

where energies are in wavenumbers and r is in angstroms. Provided that $(\epsilon_\nu/\nu)_{\max} \approx (\epsilon_\nu)_{\max}/\nu_{\max}$, which is a good approximation when $\lambda \gg k_BT$, eq 9 reduces to the Mulliken−Hush expression[21] for $(\epsilon_\nu)_{\max,i}$ (M^{-1} cm^{-1}) at $(h\nu)_{\max,i}$. Note that eqs 7 and 9 are also applicable for the case of a transition between the molecule and a single, localized site on the semiconductor surface. Within this framework, the $(\epsilon_\nu/\nu)_{\max,i}$ factors within the integrals in eqs 5 and 6 are proportional to $1/[(\nu_{\max,i})^2\sqrt{\lambda k_B T}]$ provided that $H_{12}r$ is constant.

Relative values of (ϵ_ν/ν) calculated with ρ independent of energy and assuming either $(\epsilon_\nu/\nu)_{\max,i}$ constant or replaced by the Mulliken−Hush expression (eq 9) are plotted in Figure 3. Also included is the individual Gaussian for a transition to the lowest energy level of the conduction band. An asymmetric absorption with peak at ca. $\lambda + \Delta G° + \sqrt{4\lambda k_B T}$ is predicted using the Mulliken−Hush expression with constant $H_{12}r$.

Equations 5 and 6 contain the integral of a Gaussian function multiplied by two prefactors (ρ_i and $(\epsilon_\nu/\nu)_{\max,i}$) that are both dependent on ϵ_i. The Gaussian function is relatively sharply peaked for normal values of the reorganization parameter such that, at a given value of $h\nu$ and provided that the prefactors are not strongly dependent on ϵ_i, only levels close to the level that maximizes the Gaussian, $\epsilon_{i,\max}$, contribute to the integral to any extent. For significant absorbance this maximum level is given by

$$\epsilon_{i,\max}^{CB} = -\lambda + h\nu + e(E_{bot}^{CB} - E°) \quad \text{for RBCT}$$

$$\epsilon_{i,\max}^{VB} = \lambda - h\nu + e(E_{top}^{VB} - E°) \quad \text{for BOCT} \tag{10a}$$

Under these conditions the two prefactors can be removed from inside the integral to give

$$\left(\frac{\epsilon_\nu}{\nu}\right)^{RBCT} = \rho_i^{CB}(\upsilon)\left(\frac{\epsilon_\nu}{\upsilon}\right)_{\max,i} \times \int_0^\infty \exp\left[-\frac{(\lambda - h\upsilon + \epsilon_i^{CB} - e(E_{bot}^{CB} - E^0))^2}{4\lambda k_B T}\right] d\epsilon_i^{CB} \tag{10b}$$

$$\left(\frac{\epsilon_\nu}{\nu}\right)^{BOCT} = \rho_i^{VB}(\upsilon)\left(\frac{\epsilon_\nu}{\upsilon}\right)_{\max,i} \times \int_{-\infty}^0 \exp\left[-\frac{(\lambda - h\upsilon - \epsilon_i^{VB} + e(E_{top}^{VB} - E^0))^2}{4\lambda k_B T}\right] d\epsilon_i^{VB} \tag{10c}$$

with $(\epsilon_\nu/\nu)_{\max,i}$ given by either a constant or the approximate Mulliken−Hush expression

$$\left(\frac{\epsilon_\nu}{\nu}\right)_{\max,i} = \left(\frac{7.0 \times 10^2 H_{12}{}^2 r^2}{\nu^2\sqrt{\lambda k_B T}}\right) \tag{10d}$$

and ρ_i a function of ν rather than ϵ_i. The integral of the Gaussian is given by the complementary error function[43,44,46]

$$\int_0^\infty \exp[-(\lambda - h\upsilon + \epsilon_i^{CB} - e(E_{bot}^{CB} - E^0))^2/4\lambda k_B T]\, d\epsilon_i^{CB} = \sqrt{\pi\lambda k_B T}\left[\operatorname{erfc}\left(\frac{\lambda - h\upsilon - e(E_{bot}^{CB} - E^0)}{\sqrt{4\lambda k_B T}}\right)\right] \tag{11a}$$

$$\int_{-\infty}^0 \exp[-(\lambda - h\upsilon - \epsilon_i^{VB} + e(E_{bot}^{VB} - E^0))^2/4\lambda k_B T]\, d\epsilon_i^{VB} = \sqrt{\pi\lambda k_B T}\left[\operatorname{erfc}\left(\frac{\lambda - h\upsilon + e(E_{bot}{}^{VB} - E^0)}{\sqrt{4\lambda k_B T}}\right)\right] \tag{11b}$$

Thus the following approximations are obtained

$$\left(\frac{\epsilon_\nu}{\nu}\right)^{RBCT} \propto \rho_i^{CB}(\upsilon)\left(\frac{\epsilon_\nu}{\upsilon}\right)_{\max,i}\left[\operatorname{erfc}\left(\frac{\lambda - h\upsilon - e(E_{bot}^{CB} - E^0)}{\sqrt{4\lambda k_B T}}\right)\right] \tag{11c}$$

$$\left(\frac{\epsilon_\nu}{\nu}\right)^{BOCT} \propto \rho_i^{VB}(\upsilon)\left(\frac{\epsilon_\nu}{\upsilon}\right)_{\max,i}\left[\operatorname{erfc}\left(\frac{\lambda - h\upsilon + e(E_{bot}^{VB} - E^0)}{\sqrt{4\lambda k_B T}}\right)\right] \tag{11d}$$

Relative values of (ϵ_ν/ν) calculated from eq 5 with $(\epsilon_\nu/\nu)_{\max,i}$ either constant or replaced by the Mulliken−Hush expression (eq 9) and from eq 11c with the approximate form of the Mulliken−Hush expression (eq 10d) are plotted in Figure 4 as a function of energy. The DOS was assumed constant. Also plotted are the corresponding values of ϵ_ν versus wavelength. The approximation is seen to be in good agreement with the full expression.

Magnitude of λ. The reorganization energy is comprised of inner-shell and outer-shell reorganization, λ_{in} and λ_{out}. The inner-shell or molecular reorganization derives from the changes in molecular structure that occur upon electron transfer. For a metal complex as the molecular reductant/oxidant in photoinduced interfacial charge transfer, changes in metal−ligand distances

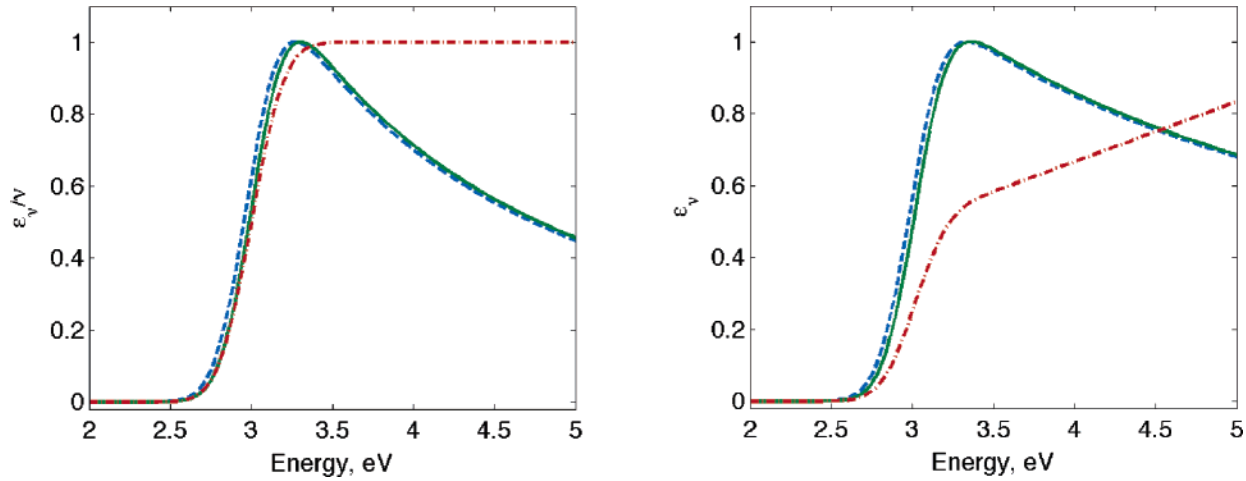

Figure 4. Relative values of (ϵ_ν/ν) calculated from eq 5 with $(\epsilon_\nu/\nu)_{\max,i}$ either constant (dash−dotted red line) or replaced by the Mulliken−Hush expression (eq 9, solid green line) and from eq 11c with the approximate form of the Mulliken−Hush expression (eq 10d, dashed blue line) plotted as a function of energy. The DOS was assumed constant. Also plotted (right-hand side) are the corresponding values of ϵ_ν vs energy.

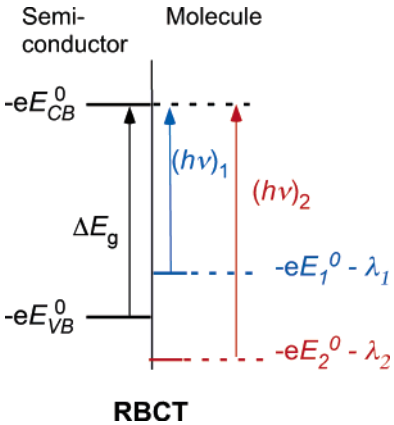

Figure 5. When the potential of the reductant couple falls in the gap between the valence and conduction bands of an n-type semiconductor (couple 1), it should be possible to discern optical RBCT.

(Δd_{ML}), force constants (f_{ML}), and angles must be included, for example

$$\lambda_{\mathrm{in}} = \sum^{\mathrm{bonds}} \frac{f_{\mathrm{ML}}^{\mathrm{D+}} f_{\mathrm{ML}}^{\mathrm{D}}}{f_{\mathrm{ML}}^{\mathrm{D+}} + f_{\mathrm{ML}}^{\mathrm{D}}} (\Delta d_{\mathrm{ML}})^2 \tag{12}$$

The outer-sphere contribution to the reorganization energy arises from the reorientation of charge in the medium. Its magnitude depends on the radius a of the molecular donor/acceptor site, on its distance d from the semiconductor, and on the dielectric properties of the donor/acceptor, the semiconductor, and the medium $(D_{\mathrm{op}}, D_{\mathrm{s}})$. For one-electron transfer between a spherical reactant and a semiconductor the medium reorganization energy is[47]

$$\lambda_{\mathrm{out}}^{\mathrm{sc}} = (\Delta q)^2 \left[\frac{1}{2a}\left(\frac{1}{D_1^{\mathrm{op}}} - \frac{1}{D_1^{\mathrm{s}}}\right) - \frac{1}{4d}\left(\frac{D_2^{\mathrm{op}} - D_1^{\mathrm{op}}}{D_2^{\mathrm{op}} + D_1^{\mathrm{op}}}\frac{1}{D_1^{\mathrm{op}}} - \frac{D_2^{\mathrm{s}} - D_1^{\mathrm{s}}}{D_2^{\mathrm{s}} + D_1^{\mathrm{s}}}\frac{1}{D_1^{\mathrm{s}}}\right)\right] \mathrm{eV} \tag{13}$$

where a and d are in nanometers, $(\Delta q)^2 = 1.44$, D_1 refers to the solvent in which the molecular donor/acceptor is immersed, and D_2 refers to the semiconductor. For water solvent and anatase $\lambda_{\mathrm{out}}^{\mathrm{sc}} \approx (\Delta q)^2\,(1/(3.6a) - 1/(12.4d))$ based on $D^{\mathrm{op}} = 1.8$ for water and $D^{\mathrm{op}} = 6.2$ and $D^{\mathrm{s}} = 85$ for TiO_2 anatase.[48]

In the case of electron transfer to/from a localized level of the semiconductor it may be more appropriate to calculate the reorganization of the surrounding medium from the expression for the reorganization energy for electron transfer across a liquid−liquid interface[47]

$$\lambda_{\mathrm{out}} = \frac{(\Delta q)^2}{2a_1}\left(\frac{1}{D_1^{\mathrm{op}}} - \frac{1}{D_1^{\mathrm{s}}}\right) + \frac{(\Delta q)^2}{2a_2}\left(\frac{1}{D_2^{\mathrm{op}}} - \frac{1}{D_2^{\mathrm{s}}}\right) - \frac{2(\Delta q)^2}{d_{12}}\left(\frac{1}{D_1^{\mathrm{op}} + D_2^{\mathrm{op}}} - \frac{1}{D_1^{\mathrm{s}} + D_2^{\mathrm{s}}}\right) + \frac{(\Delta q)^2}{4d_1}\left(\frac{D_1^{\mathrm{op}} - D_2^{\mathrm{op}}}{D_1^{\mathrm{op}}(D_1^{\mathrm{op}} + D_2^{\mathrm{op}})} - \frac{D_1^{\mathrm{s}} - D_2^{\mathrm{s}}}{D_1^{\mathrm{s}}(D_1^{\mathrm{s}} + D_2^{\mathrm{s}})}\right) - \frac{(\Delta q)^2}{4d_2}\left(\frac{D_1^{\mathrm{op}} - D_2^{\mathrm{op}}}{D_2^{\mathrm{op}}(D_1^{\mathrm{op}} + D_2^{\mathrm{op}})} - \frac{D_1^{\mathrm{s}} - D_2^{\mathrm{s}}}{D_2^{\mathrm{s}}(D_1^{\mathrm{s}} + D_2^{\mathrm{s}})}\right) \tag{14}$$

where a_1 and a_2 are the radii of the spheres in medium 1 and medium 2, respectively, d_1 and d_2 are their distances from the interface, and $d_{12} = (d_1 + d_2)$ is the distance between the two sites.

The solvent reorganization energy for charge transfer from a molecular adsorbate, modeled as a conducting sphere D of radius a_{D} separated by a distance d_{DA} from a semiconductor nanoparticle, modeled as a dielectric sphere A, in a dielectric medium (D_{s}) is given by

$$\lambda_{\mathrm{out}}^{\mathrm{DA}} = (\Delta q)^2 \left(\frac{1}{2a_{\mathrm{A}}} + \frac{1}{2a_{\mathrm{D}}} - \frac{1}{d_{\mathrm{DA}}} - \frac{1}{d_{\mathrm{DA}}^4}\left[\frac{(a_{\mathrm{A}}^3 + a_{\mathrm{D}}^3)}{2} - \frac{3D_{\mathrm{s}}^2 a_{\mathrm{A}}^3}{(2D_{\mathrm{s}} + D_{\mathrm{in,A}})^2}\right]\right)\left(\frac{1}{D_{\mathrm{op}}} - \frac{1}{D_{\mathrm{s}}}\right) \tag{15}$$

where $D_{\mathrm{in,a}}$ is the dielectric constant for sphere A.

Extension to Nanoparticles. Interfacial charge-transfer absorption is more likely to be observable for nanoparticles; the large surface area characteristic of nanoparticles maximizes the interaction of molecular adsorbates or solute molecules with the semiconductor surface. The energetics and shape of the interfacial charge-transfer absorption are expected to alter as

the size of the particle is reduced, especially into the nanometer regime;[49−51] for semiconductors the energy of the band-gap transition increases with decreasing size.[52] Further, semiconductor nanoparticles are too small to develop a space-charge layer, and as a consequence, the potential difference resulting from charge transfer to or from a redox couple in solution shows up mainly in the Helmholtz layer on the solution side, with a corresponding shift in the valence and conduction bands of the particle.[52]

Consideration of the electrostatic energy of a dielectric (D_s) sphere of radius a, with charge ze localized at its center, in a dielectric medium (D_{in}) leads to the following expressions for the valence-band ionization energy, conduction-band electron affinity, and the reduction potential for a neutral semiconductor particle[49]

$$\mathrm{IP}_r = \mathrm{IP}_\infty + \frac{(2z+1)e^2}{2a}\left[\frac{1}{D_s} - \frac{1}{D_{in}}\right] \tag{16a}$$

$$\mathrm{EA}_r = \mathrm{EA}_\infty + \frac{(2z-1)e^2}{2a}\left[\frac{1}{D_s} - \frac{1}{D_{in}}\right] \tag{16b}$$

$$E_r^0 = E_\infty^0 + \frac{(2z-1)e}{2a}\left[\frac{1}{D_s} - \frac{1}{D_{in}}\right] \tag{16c}$$

For a bulk semiconductor, in contrast to bulk metal, $\mathrm{IP}_\infty \neq \mathrm{EA}_\infty$. Consequently, depending on its charge and the relative magnitudes of D_s and D_{in}, the semiconductor particle may be more or less electron accepting or donating than the bulk material.

The above expressions consider only the Born solvation of the particle; Coulomb interaction between the electron and hole and quantum effects that become important as the particles become smaller are not taken into account. As a result the band gap calculated from eqs 16a and 16b does not show any size dependence.[53,54] The factors primarily responsible for the size dependence of the band gap are the (particle-in-a-sphere) localization energies of the hole and electron which vary as $1/a^2$; the Coulomb interaction and solvation energy both scale as $1/a$.[55,56] Moreover, since the electron−hole Coulomb interaction increases with decreasing size of the particle, it cannot account for the increase in the energy of the band-gap transition with decreasing particle size.

Density of States: Illustrated for TiO_2. Experimental[57,58] and theoretical[59,60] investigations of the DOS of anatase reveal that the valence band is composed of two sets of levels. The lower set is composed of four bands due to oxygen 2s levels and an upper set comprised of mainly oxygen 2p levels, with some Ti 3d character. The conduction band similarly consists of two regions: one below 10 eV that has mainly Ti 3d character and one above 10 eV arising from the Ti 4s- and 4p-orbitals.[59] Optical charge transfer to the various bands will have different transition moments. The DOS of rutile determined by scanning tunneling microscopy and electrochemical measurements revealed a much smaller increase in the DOS of the conduction band compared to those of the valence band.[61] The DOS of the conduction (and valence) bands change very sharply at the edges, which could significantly change the absorption profile from that presented in Figure 2.

The DOS decreases with decreasing particle size, with the particle ultimately evolving to discrete molecular orbital electronic structures in the cluster limit. Thus, in the small cluster limit, IFCTA is no longer expected to involve bands of filled and empty levels but rather HOMOs and LUMOs, and the process limits at a conventional charge-transfer process, for example, ligand-to-metal charge transfer (LMCT) if the excitation is from a ligand of the adsorbate or intervalence charge transfer (IVCT) if the excitation involves a metal redox center attached to the ligand.

III. Current Status

In 1974 Kolb et al. reported optical interfacial electron transfer from metal adatoms to electrodes of single-crystal ZnO and CdS.[30] The wavelength dependences of photocurrents introduced by Ag, Cu, and Hg monolayers were monitored between 1200 and 600 nm. For Ag on CdS, two current-plateau regions were observed in plots of log(current) versus wavelength, one at lower energy, 1.2−1.45 eV (1033−855 nm), attributed to electron transfer to empty surface states below the conduction band, and one at higher energy identified with electron transfer to the conduction band. No peaks were observed, and the photocurrent profile reported is consistent with that given by eqs 1, 5, and 11c and Figure 4b.

When is IFCTA expected to be observable? For detection of such absorption, the transition must occur at energies lower than the band gap of the semiconductor; otherwise it will be masked by the intense interband transitions. Figure 5 depicts the energetics of an n-type semiconductor and two molecular reductants 1 and 2. The reduction potential for reductant 1 lies in the gap of the semiconductor, while that of reductant 2 lies below the energy of the valence band. Thus the RBCT transition energies lie in the order $h\nu_2 > \Delta E_g > h\nu_1$, and RBCT is expected to be observable only for reductant 1 with this semiconductor. More precisely, for the Mulliken−Hush intensity mechanism, an absorption peak is at ca. $\lambda + \Delta G^\circ + \sqrt{4\lambda k_B T}$. When $\Delta E_g \geq \lambda + \Delta G^\circ + \sqrt{4\lambda k_B T}$ the absorption peak should not be obscured by the interband transition.

Recent reports of charge-transfer transitions involving semiconductors are dominated by observations on n-type titanium dioxide. In principle, such transitions should also be observed for other n-type semiconductors. The conduction bands of the metal oxides are formed from metal d-orbitals (as for TiO_2) or from s-p-orbitals (SnO, SnO_2, ZnO). For the d-type oxides, band gaps range from less than 3 eV (Fe_2O_3, MoO_3) to around 3 eV (TiO_2, Nb_2O_5) to 5 eV (ZrO_2), providing an opportunity for systematic studies of symmetry and energy dependences. Rajh[62] has reported observations for ZrO_2 and Fe_2O_3, and Lian[12,13] has begun to explore the dynamics of photoinjection as a function of the metal oxide.

The TiO_2-bound systems that exhibit new electronic absorption features are of several types. The first type contains transition-metal ions that are anchored to the surface by a bridging ligand, e.g., $(NC)_m M^{n+}$−CN. For these, the absorption has been designated metal-to-particle charge transfer (MPCT), M^{n+}-to-Ti^{4+} (to yield $M^{(n+1)+}$−CN−Ti^{3+}), analogous to IVCT in binuclear metal complexes. In the second class, the chromophore consists of organic ligands attached to the surface via the oxygen atoms of carboxylates, enediols, etc.; for these the new absorption is analogous to LMCT in character. There are other categories mentioned only briefly here: One is that of doped TiO_2, in which the origin of new electronic transitions may arise from several sources, depending on the dopant. Thus shifted absorption spectra have been reported for C- and N-doped TiO_2.[63,64] For the case of Pt-doped material, there are also new maxima in the visible region.[65] In addition, there are many colored oxide minerals in which the color is attributed to metal-to-metal (intervalence) charge transfer (MMCT) absorption,[14,15,66] for example, mixed metal oxides such as $CoTiO_3$ and $MnTiO_3$,[67] but there is little enhancement of photocurrent

for visible excitation.[67] The absorption spectra of these solids exhibit peaks and widths comparable to those seen for solutions of binuclear complexes and have been treated as pairwise features, e.g., Fe(II)−Ti(IV) to Fe(III)−Ti(III) charge transfer.[15]

To our knowledge in only one case has charge transfer in the reverse sense, i.e., excitation of a TiO_2 valence-band electron, been observed. This process has been reported for green TiO_2−MoO_3 core−shell nanoparticles.[68] In these, a TiO_2 core ranging from 4 to 9 nm in diameter is coated by n MoO_3 units (n = 0.8−1.8). The conduction band of the MoO_3 shell ($\Delta E_g \approx 2.85$ eV) is lower than the conduction band of the TiO_2 core ($\Delta E_g \approx 3.2$ eV). Thus the excitation observed is said to be due to excitation of a valence band TiO_2 electron to the MoO_3 conduction band, a core-to-shell transition. Given that the maximum coverage of MoO_3 is approximately two monolayers, it would also be reasonable to describe the transition as O_{Ti}^{2-}-to-Mo(VI) charge transfer or LMCT. Strikingly, the transition energy decreases with particle size.

Gold nanoparticles incorporated into a nanoporous TiO_2 film on an indium tin oxide glass plate inject electrons into TiO_2 upon excitation into the surface plasmon resonance (SPR) absorption band of the gold nanoparticles. The authors noted that "indirect charge transfer" (MPCT) might contribute to the absorption, the maximum of which is considerably red-shifted compared to the SPR in water or alcohol.[69]

In most of the systems considered here, only ground-state properties are considered in discussing the interactions of molecules with semiconductors. There has been far less work implicating substantial interaction between the molecular excited state and the semiconductor (exciplex). Katoh et al. have invoked exciplexes as intermediates in electron injection into several metal oxides from a range of dyes, including Ru−N3.[70] For the case of a coumarin derivative and zinc oxide, spectral data for the exciplex led to an estimated electronic coupling of 0.3 eV.[10]

Smaller than most nanoparticles (but much larger than systems for which IVCT has traditionally been studied) are metal oxide,[71−74] metal sulfide,[75−77] and metal clusters with attached donor/acceptor groups. The number of units per cluster is on the order 10^1 while in most nanoparticles studied to date this number is greater than 10^2. $M_4(SPh)_{10}^{2-}$ (donor) complexes form complexes with methyl viologen MV^{2+} (acceptor) that exhibit donot-to-acceptor charge-transfer transitions in the visible region of the spectrum.[78,79] The spectroscopy of donor/acceptor covalently attached to small clusters has been explored in only a limited way but may be expected to provide insight into IFCTA in optimized systems.

Metal Cyanides on TiO_2: Localized MMCT or Delocalized RBCT Absorption? So-called MPCT absorption was first reported for $Fe(CN)_6^{4-}$ bound to TiO_2.[5] This assignment was supported by the observation that the mixed-valence solids $Ti^{IV}M^{II}(CN)_6$, M = Ru, Fe, in which the Ti is evidently surrounded by six cyanide nitrogen atoms,[80] exhibit intense bands at ∼350 and ∼400 nm, respectively.[81] The $Fe(CN)_6^{4-}$/TiO_2 system has been studied by UV−vis,[5,81] photocurrent,[5,32,81,82] Raman,[83,84] infrared,[84−86] and electroabsorption spectroscopies[31] as well as by flash photolysis.[5−8] Computational studies recently provided support for the assignment of the transition as Fe(II)-to-TiO_2 charge transfer and attributed most of the intensity to charge transfer to the Ti(IV) to which the cyanide nitrogen is bound.[87] Such an absorption feature for the O_2Ti−NC−M assembly has also been observed[81] for M = W^{IV}, Fe^{II}, Mo^{IV}, Ru^{II}, Re^{III}, or Os^{II} and for $Fe(bpy)(CN)_4^{2-}$ (for which parallel MPCT and metal-to-ligand charge-transfer (indirect) photoinjection processes are found).[32,82] The systems studied to date are summarized in the Table 1; the absorption features may be compared with those of the Prussian blue analogues listed in Table 2.

TABLE 1: Reduction Potentials of Metal Donors and MPCT Absorption Maxima of $MTiO_2$ Assemblies

couple	$E_{1/2}$ (V) vs NHE[a]	ref	"MPCT"[a] λ_{max} (nm), (E_{op} (eV))
$Fe(CN)_6^{3-/4-}$	+0.36	32	∼420 (3.0)
$Fe(CN)_6^{3-/4-}/TiO_2$	−0.14 vs Fc (CH_3CN)	31	∼417 (3.0)
$Fe(bpy)(CN)_4^{-/2-}$	−0.62 vs Fc (CH_3CN)	32	∼420 (3.0)[b]
$Fe(bpy)(CN)_4^{-/2-}/TiO_2$	−0.19 vs Fc (CH_3CN)	32	
$Ru(CN)_6^{3-/4-}$	+0.86	88	∼350 (3.5)
$Os(CN)_6^{3-/4-}$	+0.63	88	∼350 (3.5)
$Mo(CN)_8^{3-/4-}$	+0.73		∼350 (3.5)
$W(CN)_8^{3-/4-}$	+0.46		∼360 (3.5)
$Re(CN)_7^{3-/4-}$	+0.64	89	∼380 (3.3)

[a] From ref 81, unless otherwise noted. [b] From ref 32.

TABLE 2: IVCT Bands in Mixed-Valence Hexacyanide Solids

compound	$\lambda_{max,IVCT}$ and $\Delta\nu_{1/2}$
$KFe^{III}Fe^{II}(CN)_6$	709 nm (1.75 eV)[a] $\Delta\nu_{1/2} = 6200$ cm^{-1} ($\lambda = 2.1$ eV)
$KFe^{III}Ru^{II}(CN)_6$	575 nm (2.16 eV)[a]
$KFe^{III}Os^{II}(CN)_6$	610 nm (2.03 eV)[a]
$Ti^{IV}Fe^{II}(CN)_6$	388 nm (3.20 eV)[b] $\Delta\nu_{1/2} = 6800$ cm^{-1} ($\lambda = 2.56$ eV)
$RbMn^{III}[Fe^{II}(CN)_6]$	∼700 nm[90]

[a] From ref 91. [b] Prepared as in ref 92, M. Chou, unpublished work.

Reduction potentials reported for the free cyanide complexes in water are summarized in the second column of Table 1. For the first two iron complexes, data reported for acetonitrile solvent are also included. The 430 mV cathodic shift for $Fe(bpy)(CN)_4^{-/2-}$ is noteworthy. For aqueous media the $Fe(CN)_6^{3-/4-}/TiO_2$ potential was bracketed beween +0.4 and +0.8 V vs the normal hydrogen electrode (NHE).[85] The observation of Zaban et al.[93] of pH-dependent redox potentials for adsorbed (but not free) dye molecules on films of nanoparticulate TiO_2 suggests that binding a ligand to TiO_2 may alter the redox thermodynamics of L and in a medium-dependent manner. Grätzel has given $E_{CB} = [-0.12-(0.059\ pH)]$ V vs NHE as the flat-band potential of colloidal (20 nm) TiO_2, 100−200 mV more negative than that for single-crystal rutile.[94] Ward, White, and Bard[95] estimated the reduction potential of ∼200 nm anatase TiO_2 nanoparticles at pH 6.7 to be −0.45 V vs NHE. For ligand-modified TiO_2, E_{CB} was found to be ca. 0.1 V negative of the free TiO_2.[96] These observations re-emphasize the need for direct characterization of the thermodynamics of both the nanoparticles and the attached redox couple.[97]

The MPCT absorptions in Table 1 are extremely broad, $\Delta\nu_{1/2} \approx 8000$ cm^{-1} and, in contrast to binuclear species such as $(NH_3)_5RuNCFe(CN)_5^{2-}$,[98,99] do not shift and narrow at low temperature.[31] In addition, the absorption profile does not exhibit the solvent sensitivity characteristic of the molecular dimers. Hupp has inferred a large inner-shell reorganizational energy, 0.44 eV, from resonance Raman studies.[100] The relatively large charge-transfer distance, 5.3 Å, implicated by electroabsorption studies[31] could result in a larger λ_{out} than that for the molecular

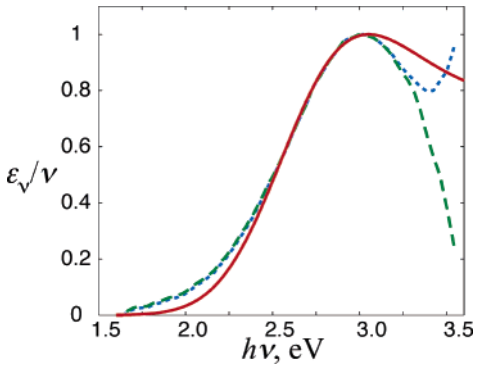

Figure 6. Comparison of observed and calculated spectra for $Fe(CN)_6^{4-}/TiO_2$ nanoparticles. The solid red line is calculated from eqs 6, 7, and 8 with $\Delta G° = 0.8$ and $\lambda = 1.8$ eV. The short-dashed blue line is a plot of the observed data,[31] and the long dashed green line is a plot of the observed data corrected for TiO_2 absorption.

species (ca. 0.5 eV based on the band narrowing observed for frozen samples[99]); 0.38 eV is calculated from eq 13. In addition, hydrogen bonding between the cyanides cis to the bridge and the O−H groups of the TiO_2 surface could contribute to the reorganization barrier and account for the solvent insensitivity of the transition.

The "MPCT" band maxima reported in Table 1 lie between approximately 380 and 480 nm (2.6 and 3.3 eV). The absorption maximum for optical electron transfer to a localized site is $E_{op} = \Delta G° + \lambda$. The vertical reorganization energy, λ, is estimated as ≤1 eV (an upper limit based on the spectra of ion pairs,[88] Yang et al. have estimated 0.3 eV[32]), and $\Delta G°$ for electron transfer from ferrocyanide to Ti^{IV} (taking $E°(Ti^{IV}/Ti^{III})$ as ∼0[101]) is ∼0.4 eV. Then the absorption maximum is estimated to be $E_{op} \leq 1.4$ eV (885 nm), much lower energy than the 2.6−3.3 eV values observed.[102] However, the intensities of the "MPCT" bands are consistent with values (typically 3000 M^{-1} cm^{-1}) reported for cyano-bridged mixed-valence complexes such as $(NC)_5Fe(\mu\text{-}CN)M'$ ($M' = Fe(CN)_5^{3-}$, $Ru(NH_3)_5^{3+}$, $Os(NH_3)_5^{3+}$), although the latter bands are much narrower, with $\Delta\nu_{1/2}$ 3000−5000 cm^{-1},[98,99] in contrast to the values of 8200 cm^{-1} reported for the first two entries in Table 1.[32] As is shown in Figure 6, the absorption profile reported in ref 31 can be simulated but with parameters, $\Delta G° = 0.8$ and $\lambda = 1.8$ eV, very different from those estimated above, although not inconsistent with the values in Table 2.

Even with $\lambda = 1.8$ eV, the weak, low-energy absorbance is not reproduced by the calculated profile. The breadth of the absorption band may in part reflect a broad dispersion in the energetics of different surface binding sites as has been implicated for catechol binding.[103]

It is also conceivable that the absorption profile contains contributions from both RBCT and MMCT. One spectral region is dominated by RBCT to sites within the nanoparticle; that is, the absorption arises from mixing with wave functions that have their electron density concentrated at the interior of the particle. In contrast, the other region is dominated by the more localized MMCT or MPCT process, with energy and intensity a result of mixing with wave functions that have maximum electron density at the surface of the particle. It is difficult to pursue this issue further without knowledge of the relative energetics of surface and interior sites. In this connection the Stark behavior of the longer-wavelength region would be of considerable interest.

Enediols on TiO_2: LMCT or RBCT Absorption. The other widely reported charge-transfer transition involving a semicon-

TABLE 3: Reduction Potentials and Reported Absorption Features for the Enediol and Other Ligands

ligand	E^0, V vs NHE[a]	λ_{max},(diameter, nm), [$\Delta\nu_{1/2}$, cm^{-1}]
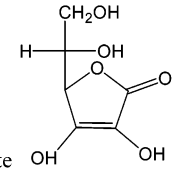 ascorbate	+0.015 (L^{2-}),[b] +0.99 LH_2 [107]	420 [108]
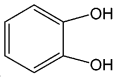 catechol	+0.043 (L^{2-})[b]; +1.06 LH_2 [107]	sh 375 (15-nm)[9200] [33] 420 nm[36] 456 nm (0.4 μ)[37] ~390 nm (6-nm)[35]
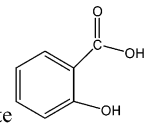 salicylate	ca +1.2 [109 c]	onset 500 nm[33] 420 nm [110]- 400 nm (Ti(IV) complex[111])
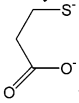 thiolactate	~1.3[112]	380 nm, 548 nm(sh)[112] ε_{380} 3.3 x 10^4 ε_{548} 1.7 x 10^3
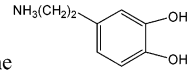 dopamine		435 nm[c]
croconate 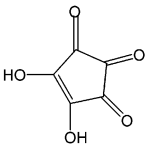		400 nm Ti(IV) complex[113]

[a] For the free ligand unless otherwise noted. [b] For the L^-/L^{2-} (deprotonated) couple.[107] [c] M. Khoudiakov, B. Brunschwig, T. Rajh, unpublished work.

ductor acceptor involves catechol and related ligands (including ascorbate[34] and DNA[104]) bound to TiO_2 nanoparticles coupled through enediol functions. Binding of these ligands to TiO_2 nanoparticles was reported to red-shift the absorption compared to those for the unmodified nanocrystallites and the free ligand. In some cases a peak was observed, and in others not. It was proposed that dihydroxycyclobutenedione shifts the optical absorption and effective band gap of TiO_2 by 0.8 eV, ascorbic acid by 1.2 eV, dopamine by 1.9 eV, *tert*-butyl catechol by 2.0 eV, and alizarine by 1.4 eV. It was concluded that,[96] upon surface modification, the positions of the Fermi level and the conduction band of TiO_2 (intrinsically n-type) are altered by ca. 0.1 eV, so the reducing properties are not changed significantly. In contrast, INDO calculations[105] suggest that in the catechol−TiO_2 (particle) system the directly injected electron goes into an orbital that has a significant contribution from the Ti 3d-orbital closest to the adsorbate with some additional contributions from other adjacent Ti centers, as do ab initio density functional theory molecular dynamics simulations.[106] The reduction potentials of bare and dopamine-capped 50 nm TiO_2 nanoparticles at pH 3.5 are −0.27 and −0.37, respectively.[96]

The structures and reduction potentials of these ligands and other adducts are given in Table 3.

An alternative description treats these absorption features as LMCT transitions. A number of computations implicate a localized acceptor state.[105,106,114,115] Such absorption features have also been reported for mononuclear Ti^{IV} complexes of catechol derivatives[116] and salicylate.[111] Lian has compared the spectra and photoinjection of catecholate-modified anatase with those of the Ti(IV) complex $Ti(cat)_3^{2-}$.[35] The complex exhibits a LMCT band at ∼400 nm. Remarkably $Ti^{IV}(cat)_3^{2-}$ has a reduction potential of −1.14 V vs NHE,[116] but its LMCT absorption (λ_{max} = 389 nm[116]) does not differ greatly from that of the catechol-capped TiO_2 materials.

IV. Concluding Remarks

In addition to an earlier report,[30] the optical charge-transfer process for $Fe(CN)_6^{4-}$ adsorbed on TiO_2 is consistent with the behavior predicted here for photoinduced charge transfer to the band levels in a semiconductor. In contrast, the absorption profiles for catechol adsorbates appear to involve localized (LMCT) transitions. The preponderance of data on nanoparticle systems leads to the conclusion that observed photoinduced charge-transfer processes involve a small number of atoms per acceptor site on the surface of the nanoparticle.

Acknowledgment. This research was carried out at Brookhaven National Laboratory under Contract No. DE-AC02-98CH10886 with the U. S. Department of Energy, supported by its Division of Chemical Sciences, Office of Basic Energy Sciences, and at the California Institute of Technology by the Arnold and Mabel Beckman Foundation. We thank T. Lian and T. Rajh for making unpublished data available to us.

References and Notes

(1) Adams, D.; Brus, L.; Chidsey, C. E. D.; Creager, S.; Creutz, C.; Kagan, C. R.; Kamat, P. V.; Lieberman, M.; Lindsay, S.; Marcus, R. A.; Metzger, R. M.; Michel-Beyerle, M. E.; Miller, J. R.; Newton, M. D.; Rolison, D. R.; Sankey, O.; Schanze, K. S.; Yardley, J.; Zhu, X. *J. Phys. Chem. B* **2003**, *107*, 6668−6697.

(2) Lewis, N. S. *J. Phys. Chem. B* **1998**, *102*, 4843−4855.

(3) Hamann, T. W.; Gstrein, F.; Brunschwig, B. S.; Lewis, N. S. *J. Am. Chem. Soc.* **2005**, *127*, 7815−7824.

(4) Hamann, T. W.; Gstrein, F.; Brunschwig, B. S.; Lewis, N. S. *J. Am. Chem. Soc.* **2005**, *127*, 13949−13954.

(5) Vrachnou, E.; Vlachopoulos, N.; Grätzel, M. *J. Chem. Soc., Chem. Commun.* **1987**, 868.

(6) Lu, H.; Prieskorn, J. N.; Hupp, J. T. *J. Am. Chem. Soc.* **1993**, *115*, 4927−4928.

(7) Ghosh, H. N.; Asbury, J. B.; Weng, Y.; Lian, T. *J. Phys. Chem. B* **1998**, *102*, 10208−10215.

(8) Weng, Y.-X.; Wang, Y.-Q.; Asbury, J. B.; Ghosh, H. N.; Lian, T. *J. Phys. Chem. B* **2000**, *104*, 93−104.

(9) Huber, R.; Sporlein, S.; Moser, J. E.; Grätzel, M.; Wachtveitl, J. *J. Phys. Chem. B* **2000**, *104*, 8995−9003.

(10) Furube, A. K., R.; Yoshihara, T.; Hara, K.; Murata, S.; Arakawa, H.; Tachiya, M. *J. Phys. Chem. B* **2004**, *108*, 12583−12592.

(11) Guo, J.; She, C.; Lian, T. *J. Phys. Chem. B* **2005**, *109*, 7095−7102.

(12) Ai, X.; Anderson, N. A.; Guo, J.; Lian, T. *J. Phys. Chem. B* **2005**, *109*, 7088−7094.

(13) Ai, X.; Guo, J. C.; Anderson, N. A.; Lian, T. Q. *J. Phys. Chem. B* **2004**, *108*, 12795−12803.

(14) Robin, M. B.; Day, P. *Adv. Inorg. Chem. Radiochem.* **1967**, *10*, 247.

(15) Allen, G. C.; Hush, N. S. *Prog. Inorg. Chem.* **1967**, *8*, 357−339.

(16) Hush, N. S. *Prog. Inorg. Chem.* **1967**, *8*, 391−444.

(17) Hush, N. S. *Electrochim. Acta* **1968**, *13*, 1005−1023.

(18) Creutz, C. *Prog. Inorg. Chem.* **1983**, *30*, 1−73.

(19) Crutchley, R. J. *Adv. Inorg. Chem.* **1994**, *41*, 273−325.

(20) Demadis, K. D.; Hartshorn, C. M.; Meyer, T. J. *Chem. Rev.* **2001**, *101*, 2655−2686.

(21) Brunschwig, B. S.; Creutz, C.; Sutin, N. *Chem. Soc. Rev.* **2002**, *31*, 168−184.

(22) Curtis, J. C.; Meyer, T. J. *J. Am. Chem. Soc.* **1978**, *100*, 6284−6286.

(23) Billing, R. *Coord. Chem. Rev.* **1997**, *159*, 257−270.

(24) Kochi, J. K.; Sun, D.; Rosokha, S. V. *J. Am. Chem. Soc.* **2004**, *126*, 1388−1401.

(25) Nelsen, S. F. *Chem.−Eur. J.* **2000**, *6*, 581−588.

(26) Lambert, C.; Noll, G. *J. Am. Chem. Soc.* **1999**, *121*, 8434−8442.

(27) Coropceanu, V.; Gruhn, N. E.; Barlow, S.; Lambert, C.; Durivage, J. C.; Bill, T. G.; Nöll, G.; Marder, S. R.; Brédas, J.-L. *J. Am. Chem. Soc.* **2004**, *126*, 2727−2731.

(28) Nelsen, S. F.; Weaver, M. N.; Konradsson, A. E.; Telo, J. P.; Clark, T. *J. Am. Chem. Soc.* **2004**, *126*, 15431−15438.

(29) Endicott, J. F.; Uddin, M. J. *Coord. Chem. Rev.* **2001**, *219*, 687−712.

(30) Kolb, D. M.; Przasnyski, M.; Gerischer, H. *Z. Phys. Chem. Neue Folge* **1974**, *93*, 1−14.

(31) Khoudiakov, M.; Parise, A. R.; Brunschwig, B. S. *J. Am. Chem. Soc.* **2003**, *125*, 4637−4642.

(32) Yang, M.; Thompson, D. W.; Meyer, G. J. *Inorg. Chem.* **2002**, *41*, 1254−1262.

(33) Moser, J.; Punchihewa, S.; Infelta, P. P.; Grätzel, M. *Langmuir* **1991**, *7*, 3012−3018.

(34) Rajh, T.; Nedeljkovic, J. M.; Chen, L. X.; Poluektov, O.; Thurnauer, M. C. *J. Phys. Chem. B* **1999**, *103*, 3515−3519.

(35) Wang, Y.; Hang, K.; Anderson, N. A.; Lian, T. *J. Phys. Chem. B* **2003**, *107*, 9434−9440.

(36) Rodriguez, R.; Blesa, M. A.; Regazzoni, A. E. *J. Colloid Interface Sci.* **1996**, *177*, 122−131.

(37) Liu, Y. M.; Dadap, J. I.; Zimdars, D.; Eisenthal, K. B. *J. Phys. Chem. B* **1999**, *103*, 2480−2486.

(38) Klimov, V. I.; Schwarz, C. J.; McBranch, D. W.; Leatherdale, C. A.; Bawendi, M. G. *Phys. Rev. B* **1999**, *60*, R2177−R2180.

(39) Blackburn, J. L.; Ellingson, R. J.; Micic, O. I.; Nozik, A. J. *J. Phys. Chem. B* **2003**, *107*, 102−109.

(40) Tu, H. H.; Mogyorosi, K.; Kelley, D. F. *Phys. Rev. B* **2005**, *72*, 205306 and references therein.

(41) Hush, N. S. *J. Electroanal. Chem.* **1999**, *460*, 5−29.

(42) Hush, N. S. *J. Electroanal. Chem.* **1999**, *470*, 170−195.

(43) Creutz, C.; Brunschwig, B. S.; Sutin, N. *Chem. Phys.* **2006**, *324*, 244−258.

(44) Creutz, C.; Brunschwig, B. S.; Sutin, N. *J. Phys. Chem B* **2005**, *109*, 10251−10260.

(45) Atkins, P. W.; Friedman, R. S. *Molecular Quantum Mechanics*, 3rd ed.; Oxford University Press: Oxford, U. K., 1997; p 509.

(46) In part 1 of this series,[44] the term $\sqrt{4\lambda k_B T}$ was omitted in the prefactor and in the denominator of the argument of the error function expressions in eqs 28b and 29b. However, the absorbance profiles shown were calculated from the correct expressions.

(47) (a) Marcus, R. A. *J. Phys. Chem.* **1990**, *94*, 1050−1055. (b) Kharkats, Y. I. *Sov. Electrochem.* **1976**, *12*, 1257−1263. (c) German, E. D.; Kuznetsov, A. M. *Electrochim. Acta* **1981**, *26*, 1595−1608.

(48) Parker, R. A. *Phys. Rev.* **1961**, *124*, 1719.

(49) Creutz, C.; Brunschwig, B. S.; Sutin, N. In *Comprehensive Coordination Chemistry II*; McLeverty, J., Meyer, T. J., Eds.; Elsevier: Amsterdam, 2004; Vol. 7, pp 731−777.

(50) Jortner, J. *Z. Phys. D* **1992**, *24*, 247−275.

(51) Ratner, M. A.; Jortner, J. In *Molecular Electronics*; Ratner, M. A., Jortner, J., Eds.; Blackwell: Oxford, U. K., 1997; pp 5−72 and references therein.

(52) Hagfeldt, A.; Grätzel, M. *Chem. Rev.* **1995**, *95*, 49−68.

(53) The band gap of a semiconductor is the (photon) energy required to promote an electron from the valence band to the conduction band with the electron and hole produced at rest with respect to the lattice.[54] To show that the Born solvation change is not responsible for the size dependence of the band gap, the VB-to-CB transition may be viewed as a (hypothetical) two-step process with the ionization of the particle of charge $+ze$ yielding a particle of charge $+(z + 1)e$, which then undergoes electron capture to reform the particle of charge $+ze$. Since the band gap is equal to the difference between the ionization potential and the electron affinity of the particle, eqs 15a and 15b yield the following expressions for the dependence of the band gap of a spherical particle on the solvation change

$$(\Delta E_g)_r = (\Delta E_g)_\infty + [(\mathrm{IP})_r - (\mathrm{IP})_\infty] - [(\mathrm{EA})_r - (\mathrm{EA})_\infty]$$
$$= (\Delta E_g)_\infty + [(2z + 1) - \{2(z + 1) - 1\}]e^2/2a[1/D_s - 1/D_{in}]$$

Evidently the increase in solvation energy upon ionization is exactly canceled by the decrease in solvation energy upon electron capture resulting in $(\Delta E_g)_r = (\Delta E_g)_\infty$. This Born solvation-energy independence is hardly surprising since the charge of the semiconductor (in contrast to its internal charge distribution, which also affects the solvation energy and which is neglected here) does not change in a band-gap transition.

(54) Brus, L. E. *J. Chem. Phys.* **1984**, *80*, 4403−4409.

(55) Brus, L. *J. Phys. Chem.* **1986**, *90*, 2555−2560.

(56) Norris, D. J.; Bawendi, M. G.; Brus, L. E. In *Molecular Electronics*; Ratner, M. A., Jortner, J., Eds.; Blackwell: Oxford, U. K., 1997; pp 281−323.

(57) Sanjines, R.; Tang, H.; Berger, H.; Gozzo, F.; Margaritondo, G.; Levy, F. *J. Appl. Phys.* **1994**, *75*, 2945−2951.

(58) Degroot, F. M. F.; Faber, J.; Michiels, J. J. M.; Czyzyk, M. T.; Abbate, M.; Fuggle, J. C. *Phys. Rev. B* **1993**, *48*, 2074−2080.

(59) Calatayud, M.; Mori-Sanchez, P.; Beltran, A.; Pendas, A. M.; Francisco, E.; Andres, J.; Recio, J. M. *Phys. Rev. B* **2001**, *64*, 184113.

(60) Asahi, R.; Taga, Y.; Mannstadt, W.; Freeman, A. J. *Phys. Rev. B* **2000**, *61*, 7459−7465.

(61) Casillas, N.; Snyder, S. R.; Smyrl, W. H.; White, H. S. *J. Phys. Chem.* **1991**, *95*, 7002−7007.

(62) Rajh, T.; Chen, L. X.; Lukas, K.; Liu, T.; Thurnauer, M. C.; Tiede, D. M. *J. Phys. Chem. B* **2002**, *106*, 10543−10552.

(63) Torres, G. R.; Lindgren, T.; Lu, J.; Granqvist, C.-G.; Lindquist, S.-E. *J. Phys. Chem. B* **2004**, *108*, 5995−6003.

(64) Mrowetz, M.; Balcerski, W.; Colussi, A. J.; Hoffmann, M. R. *J. Phys. Chem. B* **2004**, *108*, 17269−17273.

(65) Kim, S.; Hwang, S.-J.; Choi, W. *J. Phys. Chem. B* **2005**, *109*, 24260−24267.

(66) Townsend, M. G. *Solid State Commun.* **1968**, *6*, 81−83.

(67) De Haart, L. G. J.; De Vries, A. J.; Blasse, G. *Mater. Res. Bull.* **1984**, *19*, 817−824.

(68) Elder, S. H.; Cot, F. M.; Su, Y.; Heald, S. M.; Tyryshkin, A. M.; Bowman, M. K.; Gao, Y.; Joly, A. G.; Balmer, M. L.; Kolwaite, A. C.; Magrini, K. A.; Blake, D. M. *J. Am. Chem. Soc.* **2000**, *122*, 5138−5146.

(69) Tian, Y.; Tatsuma, T. *J. Am. Chem. Soc.* **2005**, *127*, 7632−7637.

(70) Katoh, R. F., A.; Yoshihara, T.; Hara, K.; Fujihashi, G.; Takano, S.; Murata, S.; Arakawa, H.; Tachiya, M. *J. Phys. Chem. B* **2004**, *108*, 4818−4822.

(71) Meiklejohn, P. T.; Pope, M. T.; Prados, R. A. *J. Am. Chem. Soc.* **1974**, *96*, 6779−6781.

(72) Stark, J. L.; Young, V. G., Jr.; Maatta, E. A. *Angew. Chem., Int. Ed. Engl.* **1995**, *34*, 2547.

(73) Kang, J.; Nelson, J. A.; Lu, M.; Xie, B.; Peng, Z.; Powell, D. R. *Inorg. Chem.* **2004**, *43*, 6408−6413.

(74) Dablemont, C. P., A.; Thouvenot, R.; Afonso, C.; Fournier, F.; Tabet, J.-C. *Inorg. Chem.* **2004**, *43*, 3514−3520.

(75) Yoon, D. I.; Selmarten, D. C.; Lu, H.; Liu, H. J.; Mottley, C.; Ratner, M. A.; Hupp, J. T. *Chem. Phys. Lett.* **1996**, *251*, 84−89.

(76) Herron, N.; Suna, A.; Wang, Y. *J. Chem. Soc., Dalton Trans.* **1992**, 2329−2335.

(77) Liu, H.-J.; Hupp, J. T.; Ratner, M. A. *J. Phys. Chem.* **1996**, *100*, 12204−12213.

(78) Tuerk, T.; Resch, U.; Fox, M. A.; Vogler, A. *J. Phys. Chem.* **1992**, *31*, 1854−1857.

(79) Tuerk, T.; Resch, U.; Fox, M. A.; Vogler, A. *J. Phys. Chem.* **1992**, *96*, 3818−3822.

(80) Kemp Maer, J.; Beasley, M. L.; Collins, R. L.; Milligan, W. O. *J. Am. Chem. Soc.* **1968**, *90*, 3201−3208.

(81) Vrachnou, E.; Gratzel, M.; McEvoy, A. J. *J. Electroanal. Chem.* **1989**, *258*, 193−205.

(82) Yang, M.; Thompson, D. W.; Meyer, G. J. *Inorg. Chem.* **2000**, *39*, 3738−3739.

(83) Blackbourn, R. L.; Johnson, C. S.; Hupp, J. T. *J. Am. Chem. Soc.* **1991**, *113*, 1060−1062.

(84) Umapathy, S.; McQuillan, A. J.; Hester, R. E. *Chem. Phys. Lett.* **1990**, *170*, 128−132.

(85) Desilvestro, J.; Pons, S.; Vrachnou, E.; Gratzel, M. *J. Electroanal. Chem.* **1988**, *246*, 411−422.

(86) Dobson, K. D.; McQuillan, A. J. *Phys. Chem. Chem. Phys.* **2000**, *2*, 5180−5188.

(87) Angelis, F. D.; Tilocca, A.; Selloni, A. *J. Am. Chem. Soc.* **2004**, *126*, 15024−15025.

(88) Billing, R.; Vogler, A. *J. Photochem. Photobiol., A* **1997**, *103*, 239−247.

(89) Marty, W.; Renaud, P.; Gampp, H. *Helv. Chim. Acta* **1987**, *70*, 375−380.

(90) Tokoro, H.; Ohkoshi, S.; Matsuda, T.; Hashimoto, K. *Inorg. Chem.* **2004**, *43*, 5231−5236.

(91) Robin, M. B. *Inorg. Chem.* **1962**, *1*, 337−342.

(92) Maer, K. J.; Beasley, M. L.; Collins, R. L.; Milligan, W. O. *J. Am. Chem. Soc.* **1968**, *90*, 3201−3208.

(93) Zaban, A.; Ferrere, S.; Gregg, B. A. *J. Phys. Chem. B* **1998**, *102*, 452−460.

(94) Duonghong, D.; Ramsden, J.; Grätzel, M. *J. Am. Chem. Soc.* **1982**, *104*, 2977−2985.

(95) Ward, M. D.; White, J. R.; Bard, A. J. *J. Am. Chem. Soc.* **1983**, *105*, 27−31.

(96) Dimitrijevic, N. M.; Saponjic, Z. V.; Bartels, D. M.; Thurnauer, M. C.; Tiede, D. M.; Rajh, T. *J. Phys. Chem. B* **2003**, *107*, 7368−7375.

(97) Is there ground-state charge transfer from Fe^{II} to the particle? Vibrational spectroscopy of the complexed TiO_2 indicates that charge transfer is substantial. For the separated species, with $E_{CB}(TiO_2) \approx 0$ V vs NHE and $E°(Fe(CN)_6^{3-/4-}) = +0.4$ V vs NHE, the equilibrium constant for the electron transfer between the separated pair $(TiO_2)_{aq,n} + Fe(CN)_6^{4-}$,

$$(TiO_2)_{aq,1} + FeCN_6^{4-} \rightleftharpoons (TiO_2)^-_{aq,1} + Fe(CN)_6^{3-} \quad K_{17} \tag{17}$$

K_{17}, is ca. 10^{-5}. For a 5 nm TiO_2 particle, ca. 10% of the titania sites bind $Fe(CN)_6^{4-}$ so that the effective value for K_{17} is an order of magnitude greater. Thus one expects oxidation of 1 in 10 000 ferrocyanide ions. This estimate is for the separated ions and certainly underestimates the reduction potential of $Fe(CN)_6^{4-}$, which is greatly stabilized over that of Fe(III) by binding to $(TiO_2)_{aq,n}$. Indeed, there is no spectroscopic evidence for significant doping of the TiO_2.

(98) Dong, Y.; Hupp, J. T. *Inorg. Chem.* **1992**, *31*, 3322−3324.

(99) Vance, F. W.; Karki, L.; Reigle, J. K.; Hupp, J. T.; Ratner, M. A. *J. Phys. Chem. A* **1998**, *102*, 8320−8324.

(100) Hupp, J. T.; Williams, R. D. *Acc. Chem. Res.* **2001**, *34*, 808−817.

(101) Clark, W. D. K.; Sutin, N. *J. Am. Chem. Soc.* **1977**, *99*, 4676−4682.

(102) We have considered an alternative assignment of cyanide-to-Ti^{IV} for this transition: Indeed the positions of the relatively intense bands ($\epsilon = 1$ to 5×10^3 M^{-1} cm^{-1} per adsorbed M(CN) complex[78]) are typical of LMCT NC^--to-M^{n+1} transitions (to yield $NC-M^n$ where CN is the neutral cyanogen radical). LMCT band maxima for $M(CN)_6^{3-}$ are given in the fifth column of the table. Indeed it is reasonable to assign the $Fe(CN)_6^{4-}/TiO_2$ etc. bands to LMCT as well, with the transition due to excitation of an electron from cyanide to Ti^{IV} (or the conduction band), i.e., $M^{n+}-{}^-CN-Ti^{4+}$ to $M^{n+}-CN-Ti^{3+}$. $RbMn[Fe(CN)_6]$ contains Mn^{II} and Fe^{III} at high temperature and at low temperature isomerizes to Mn^{III} and Fe^{II}. Absorptions near 410 and 520 nm in the high-temperature phase are due to a LMCT of $[Fe^{III}(CN)_6]$ and d−d transition of Fe^{III} ($^2T_{2g}$ $^4T_{1g}$), respectively. In the low-temperature phase, the absorptions around 540 nm ($^5B_{1g}$ $^5B_{2g}$, ^5E_g) and 1100 nm ($^5B_{1g}$, $^5A_{1g}$) are due to Jahn−Teller distorted Mn^{III},[20] and the broad absorption around 700 nm is from the metal-to-metal charge-transfer band (intervalence-transfer band) in the mixed-valence compound.[90]

(103) Pan, D.; Hu, D.; Lu, H. P. *J. Phys. Chem. B* **2005**, *109*, 16390−16395.

(104) Rajh, T.; Saponjic, Z.; Liu, J.; Dimitrijevic, N. M.; Scherer, N. F.; Vega-Arroyo, M.; Zapol, P.; Curtiss, L. A.; Thurnauer, M. C. *Nano Lett.* **2004**, *4*, 1017−1023.

(105) Persson, P.; Bergstrom, R.; Lunell, S. *J. Phys. Chem. B* **2000**, *104*, 10348−10351.

(106) Rego, L. G. C.; Batista, V. S. *J. Am. Chem. Soc.* **2003**, *125*, 7989−7997.

(107) Steenken, S.; Neta, P. *J. Phys. Chem.* **1979**, *83*, 1134−1137.

(108) Xagas, A. P.; Bernard, M. C.; Hugot-Le Goff, A.; Spyrellis, N.; Loizos, Z.; Falaras, P. *J. Photochem. Photobiol., A* **2000**, *132*, 115−120.

(109) Constantino, V. R. L.; Toma, H. E.; Oliveira, L. F. C. d.; Rein, F. N.; Rocha, R. C.; Silva, D. d. O. *J. Chem. Soc., Dalton Trans.* **1999**, 1735−1740.

(110) Regazzoni, A. E.; Mandelbaum, P.; Matsuyoshi, M.; Schiller, S.; Bilmes, S. A.; Blesa, M. A. *Langmuir* **1998**, *14*, 868−874.

(111) Hultquist, A. E. *Anal. Chem.* **1964**, *36*, 149−151.

(112) Thurnauer, M. C.; Rajh, T.; Tiede, D. M. *Acta Chem. Scand.* **1997**, *51*, 610−618.

(113) Noda, L. K.; Goncalves, N. S.; Santos, P. S.; Sala, O. *J. Braz. Chem. Soc.* **1996**, *7*, 385−390.

(114) Duncan, W. R.; Prezhdo, O. V. *J. Phys. Chem B* **2005**, *109*, 17998−18002.

(115) Stier, W.; Prezhdo, O. V. *J. Phys. Chem. B* **2002**, *106*, 8047−8054.

(116) Borgias, B. A.; Cooper, S. R.; Koh, Y. B.; Raymond, K. N. *Inorg. Chem.* **1984**, *23*, 1009−1016.